Reactions of Di- and Polynuclear Complexes. 11.[1] The Alkyne Interaction: Kinetic and Electrochemical Study on the Parallel μ_3-η^2 Bonding Mode in Trinuclear Carbonyl Clusters of Iron. Influence of External Ligands on the Alkyne Orientation in $[Fe_3Cp_2(CO)_5(CF_3C_2CF_3)]$

René Rumin, Françoise Robin-Le Guen, Jean Talarmin, and François Y. Pétillon*

URA CNRS No. 322, "Chimie, Electrochimie Moléculaires et Chimie Analytique", Faculté des Sciences, Université de Bretagne Occidentale, BP 809, 29285 Brest Cédex, France

Received October 5, 1993®

The parallel μ_3-η^2 alkyne–cluster interaction in triiron compounds of the formula $[Fe_3Cp_2(CO)_5(CF_3C_2CF_3)]$ (**1**) has been investigated. Kinetics of the interconversion of asymmetrical (**1a**) and symmetrical (**1b**) conformers are reported. The influence of external ligands on the alkyne orientation is examined on treating **1** with tertiary phosphine and phosphite. The monosubstituted complexes $[Fe_3Cp_2(CO)_4(L)(CF_3C_2CF_3)]$ (L = PMe_3 (**2**), $P(OMe)_3$ (**3**)), in which the alkyne ligand is bonded in a μ_3-$\eta^2(\|)$ mode, are obtained. The redox chemistry of triiron alkyne clusters **1**–**3** has been investigated by electrochemical techniques. One-electron reduction coupled with the decoordination of a ligand (CO or phosphorus ligand) induces alkyne reorientation over the trimetallic framework.

Introduction

The structures and bonding aspects of trinuclear metal–alkyne clusters have been the subject of many recent publications.[2] These M_3C_2 compounds are known to adopt two different geometries, depending on their number of valence electrons. Whereas the alkyne C–C vector is perpendicular to a metal–metal bond (μ_3-$\eta^2(\perp)$ mode[3]) in the formally unsaturated 46-electron closo clusters, it is parallel to a M–M bond (μ_3-$\eta^2(\|)$ mode[3]) in 48-electron nido M_3C_2 species.[2a,b,3,4]

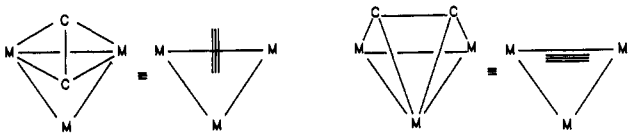

μ_3-$\eta^2(\perp)$ μ_3-$\eta^2(\|)$

In an extended Hückel molecular orbital (EHMO) study, Saillard and co-workers[2b] have shown that the μ_3-$\eta^2(\perp)$ configuration is favored by ~63 kJ mol^{-1} for 46 electrons but that the μ_3-$\eta^2(\|)$ mode is preferred by ~138 kJ mol^{-1} for 48 electrons; this is a consequence of the different energies of the frontier orbitals. The same behavior had been predicted before by Schilling and Hoffmann.[4] Aime and co-workers[2c] have confirmed these theoretical results by CNDO calculations, and they have rationalized the tendency of triiron clusters to give 46-electron systems and of triruthenium and triosmium clusters to afford 48-electron compounds when reacted with alkynes on the basis of the different electronegativities of the metals. Thus, as expected, the μ_3-$\eta^2(\perp)$ mode has been experimentally observed for $[Fe_3(CO)_9(RC_2R)]$[2h,5] and $[Fe_2Ru(CO)_9(RC_2R)]$,[6] while the μ_3-$\eta^2(\|)$ mode is observed in triruthenium[7] and triosmium[2c,f,k,8] M_3C_2 complexes and in several heterometallic cluster–alkyne compounds.[2e,i,8] However, we[2g,l] and others[2f,n] have recently reported two important exceptions to this general trend. Indeed, Smith and co-workers[2f] have described the first structurally characterized example of the μ_3-$\eta^2(\perp)$ coordination mode of an alkyne to an Os_3 framework. They explained the formation of such a complex by an increase of the electronic density onto two osmium atoms by replacement of CO with a diphosphine ligand, which allows these metal atoms to act as good back-donors to the alkyne ligand, thus stabilizing the μ_3-$\eta^2(\perp)$ coordination mode. Recently, we have presented unprecedented evidence for the existence

• Abstract published in *Advance ACS Abstracts*, February 15, 1994.

(1) Rumin, R.; Robin-Le Guen, F.; Pétillon, F. Y.; Pichon, R.; Talarmin, J. *Organometallics* **1993**, *12*, 1597.

(2) (a) Sappa, E.; Tiripicchio, A.; Braunstein, P. *Coord. Chem. Rev.* **1985**, *65*, 219 and references cited therein. (b) Halet, J. F.; Saillard, J.-Y.; Lissilour, R.; McGlinchey, M. J.; Jaouen, G. *Inorg. Chem.* **1985**, *24*, 218. (c) Aime, S.; Bertoncello, R.; Busetti, V.; Gobetto, R.; Granozzi, G.; Osella, D. *Inorg. Chem.* **1986**, *25*, 4004. (d) Osella, D.; Gobetto, R.; Montangero, P.; Zanello, P.; Cinquantini, A. *Organometallics* **1986**, *5*, 1247. (e) Einstein, F. W. B.; Tyers, K. G.; Tracey, A. S.; Sutton, D. *Inorg. Chem.* **1986**, *25*, 1631. (f) Clucas, J. A.; Dolby, P. A.; Harding, M. M.; Smith, A. K. *J. Chem. Soc., Chem. Commun.* **1987**, 1829. (g) Rumin, R.; Pétillon, F. Y.; Henderson, A. H.; Manojlović-Muir, Lj.; Muir, K. W. *J. Organomet. Chem.* **1987**, *336*, C50. (h) Carty, A. J.; Taylor, N. J.; Sappa, E. *Organometallics* **1988**, *7*, 405. (i) Boccardo, D.; Botta, M.; Gobetto, R.; Osella, D.; Tiripicchio, A.; Tiripicchio-Camellini, M. *J. Chem. Soc., Dalton Trans.* **1988**, 1249. (j) Rosenberg, E.; Bracker-Novak, J.; Gellert, R. W.; Aime, S.; Gobetto, R.; Osella, D. *J. Organomet. Chem.* **1989**, *365*, 163. (k) Gallop, M. A.; Johnson, B. F. G.; Khattar, R.; Lewis, J.; Raithby, P. R. *J. Organomet. Chem.* **1990**, *386*, 121. (l) Rumin, R.; Pétillon, F. Y.; Manojlović-Muir, Lj.; Muir, K. W. *Organometallics* **1990**, *9*, 944. (m) Aime, S.; Gobetto, R.; Milone, L.; Osella, D.; Violano, L.; Arce, A. J.; De Sanctis, Y. *Organometallics* **1991**, *10*, 2854. (n) Rivomanana, S.; Lavigne, G.; Lugan, N.; Bonnet, J. J. *Inorg. Chem.* **1991**, *30*, 4110. (o) Deeming, A. J.; Senior, A. M. *J. Organomet. Chem.* **1992**, *439*, 177.

(3) Thomas, M. G.; Muetterties, E. L.; Day, R. O.; Day, V. W. *J. Am. Chem. Soc.* **1976**, *98*, 4645.

(4) Schilling, B. E. R.; Hoffmann, R. *J. Am. Chem. Soc.* **1979**, *101*, 3456.

(5) Blount, J. F.; Dahl, L. F.; Hoogzand, C.; Hübel, W. *J. Am. Chem. Soc.* **1966**, *88*, 292.

(6) Busetti, V.; Granozzi, G.; Aime, S.; Gobetto, R.; Osella, D. *Organometallics* **1984**, *3*, 1510.

(7) (a) Hardcastle, K. I.; McPhilipps, T.; Arce, A. J.; De Sanctis, Y.; Deeming, A. J.; Powell, N. I. *J. Organomet. Chem.* **1990**, *389*, 361. (b) Rivomanana, S.; Lavigne, G.; Lugan, N.; Bonnet, J. J. *Organometallics* **1991**, *10*, 2285.

(8) (a) Deeming, A. J.; Kimber, R. E.; Underhill, M. *J. Chem. Soc., Dalton Trans.* **1973**, 2589. (b) Tachikawa, M.; Shapley, J. R.; Pierpont, C. G. *J. Am. Chem. Soc.* **1975**, *97*, 7172. (c) Clauss, A. D.; Shapley, J. R.; Wilson, S. R. *J. Am. Chem. Soc.* **1981**, *103*, 7387.

0276-7333/94/2313-1155$04.50/0

of the μ_3-$\eta^2(\|)$ mode in a triiron monoalkyne cluster, $[Fe_3Cp_2(CO)_5(CF_3C_2CF_3)]$ (**1**).[2g,l] It appears that the above change of alkyne orientation in triiron–alkyne complexes results from the influence of the substituents on the alkyne.

Within the μ_3-$\eta^2(\|)$ coordination mode, two possible conformations of nido clusters can occur when the symmetry of the triangular metallacycle is lowered either by use of different metals (M_2M') or by varying the environment of the metals. Both symmetrical (MM//C–C) and asymmetrical (MM'//C–C) geometries have been described for several nido M_2M'–alkyne complexes.[2] EHMO calculations on nido clusters by Saillard and coworkers[2b] suggest that the thermodynamically preferred rotamer is the one having the more electronegative metal fragments located in the basal edge rather than in the apical vertex of the complex. On the basis of their calculations, these authors predicted, for example, that for the two nido isomers of $[Fe_3Cp_2(CO)_3(C_2H_2)]^{4-}$ the symmetrical form is more stable than the asymmetrical one.[2b] This preferred orientation of the alkyne results from the relevant role of the cluster–alkyne back-donation from the two equivalent electron-attracting CpFe fragments. Although the difference in energy of the two possible isomers has been evaluated to be small,[2b] it could be considered to be significant enough, since the configurations studied in the theoretical work have been exemplified by several structures.[2,9] The available X-ray structures for most of the cited homo- or heterotrimetallic clusters are in good agreement with these features and show that the basal metal–C(alkyne) distances are on average shorter than the apical metal–C distance.[2j,k,8,10]

The triiron alkyne cluster $[Fe_3Cp_2(CO)_5(CF_3C_2CF_3)]$ (**1**), which we reported recently,[2g,l] should have experimentally exemplified the preferred conformers predicted by EHMO calculations for a "$Cp_2Fe_2Fe(CO)_3$" entity.[2b] Surprisingly, both in solution and in the solid state, the asymmetrical conformation **1a** is preferred to the symmetrical **1b**. Moreover, the relative energies of **1a** and **1b** are sufficiently differentiated to allow for only isomer **1a** to exist in the crystal. These results illustrate that slight changes in the coordination sphere of the triiron "$Cp_2Fe_2Fe(CO)_3$" framework would stabilize the structure calculated to be unfavored **2b**. This is particularly true when the energetic difference between the two conformers is small.

We report here a quantitative investigation of the kinetics of the asymmetrical to symmetrical conformer interconversion (**1a** ⇌ **1b**). In order to evaluate the electronic influence of external ligands on the alkyne orientation, we have brought about the substitution of one CO group in $[Fe_3Cp_2(CO)_5(CF_3C_2CF_3)]$ (**1**) by trimethyl phosphite and trimethylphosphine. Moreover, it has been previously demonstrated that the two-electron reduction of the 46-electron $[Fe_3(CO)_9(RCCR)]$ species induces a reorientation of the alkyne moiety above the metal triangle.[2d] We thought that it would be interesting to check whether the same type of chemistry could result

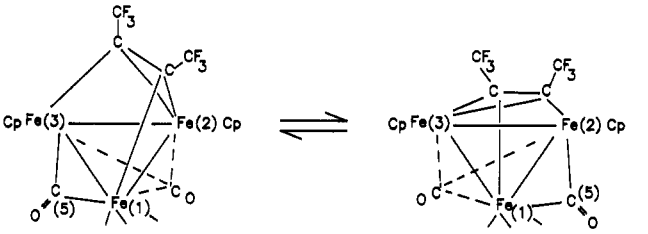

1a **1b**

from the electroreduction of the title clusters; a previous study from this laboratory showed that the reduction of a "Fe_2SC_2" nido complex triggered the decoordination of a CO group, thus generating an unsaturated 17-electron iron center.[11] If the same holds true for the title compounds, the one-electron reduction of the nido clusters[2l] could generate the radical anion of a closo species *via* the decoordination of a two-electron-donor ligand.

Results and Discussion

Kinetics of the Isomerization. The complex $[Fe_3Cp_2(CO)_5(CF_3C_2CF_3)]$ (**1**) studied here exists in solution as interconverting asymmetrical (**1a**) and symmetrical (**1b**) isomers. The **1a**:**1b** ratios are temperature-independent but depend on the solvent polarity; the more polar solvent favors the asymmetrical isomer (e.g., **1a**:**1b** = 7:1 in CD_2Cl_2 and 13:1 in CD_3CN). The asymmetrical compound **1a**, which is thermodynamically favored in the solvents used, is the only product obtained in the solid state. CD_2Cl_2 solutions of **1a**, at 200 K, display a single ^{19}F NMR pattern in accordance with the structure found for this cluster by an X-ray crystallographic study.[2g] Under the above-mentioned conditions, **1a** isomerizes over several days to give an equilibrium mixture of **1a** and **1b** in the ratio of 7:1. The conversion of **1a** to **1b** could occur according to a mechanism (Scheme 1) similar to that suggested by Deeming for the isomerization of the triosmium cluster $[Os_3H_2(\mu_3\text{-indyne})(CO)_9]$.[12] This mechanism involves an intermediate (**1c**) where the C–C axis of the alkyne is perpendicular to a metal–metal edge of the Fe_3 triangle. To account for this scheme, we have to invoke both alkyne rotation and migration of the bridging C(5)O ligand in **1a** from one edge of the Fe_3 triangle to another. In this case the Fe(1)–C(5) bond would be broken, which would be consistent with the X-ray results that indicate this bond is weak (2.23(1) Å) compared with the Fe(3)–C(5) bond (1.79(1) Å).[2g] The exchange process that is responsible for the **1a** → **1b** interconversion is thought to be slow, since no fluxional phenomena could be detected on the NMR (^{19}F, ^{13}C) time scale, over the temperature range 200–383 K in toluene-d_8. Therefore, to know more about the energy differential in the transformation of complex **1a** to **1b** and vice versa, we studied the kinetics of the isomerization reaction

$$\mathbf{1a} \underset{k_{-1}}{\overset{k_1}{\rightleftharpoons}} \mathbf{1b} \qquad (1)$$

Rates for reaction 1 were monitored by following changes in the ^{19}F NMR spectra with time, at four temperatures. The rate constants are given in Table 1 and were obtained

(9) (a) Shapley, J. R.; Park, J. T. *J. Am. Chem. Soc.* **1981**, *103*, 7385. (b) Aime, S.; Milone, L.; Osella, D.; Tiripicchio, A.; Manotti-Lanfredi, A. M. *Inorg. Chem.* **1982**, *21*, 501. (c) Busetto, L.; Green, M.; Hessner, B.; Howard, J. A. K.; Jeffery, J. C.; Stone, F. G. A. *J. Chem. Soc., Dalton Trans.* **1983**, 519. (d) Mlekuz, M.; Bougeard, P.; Sayer, B. G.; Peng, S.; McGlinchey, M. J.; Marinetti, A.; Saillard, J. Y.; Ben Naceur, J.; Mentzen, B.; Jaouen, G. *Organometallics* **1985**, *4*, 1123.

(10) (a) Deeming, A. J.; Rothwell, I. P.; Hursthouse, M. B.; Backer-Dirks, J. D. J. *J. Chem. Soc., Dalton Trans.* **1981**, 1879. (b) Sappa, E.; Manotti-Lanfredi, A. M.; Tiripicchio, A. *J. Organomet. Chem.* **1981**, *221*, 93.

(11) Robin, F.; Rumin, R.; Talarmin, J.; Pétillon, F. Y.; Muir, K. W. *Organometallics* **1993**, *12*, 365.

(12) Deeming, A. J. *J. Organomet. Chem.* **1978**, *150*, 123.

Scheme 1

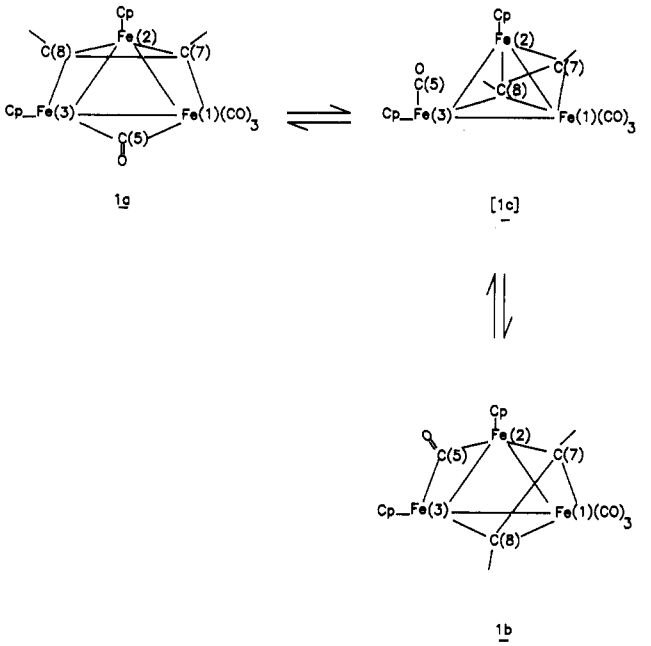

Table 1. Temperature Dependence of k_1 and k_{-1} for 1a–1b Isomerization (0.2 M) in $CDCl_3$

temp, K	$k_{-1} \times 10^4$, s^{-1}	$k_1 \times 10^4$, s^{-1}	temp, K	$k_{-1} \times 10^4$, s^{-1}	$k_1 \times 10^4$, s^{-1}
269	1.33	1.90	279.5	5.12	7.32
275	2.65	3.79	285	9.80	14

from the slopes of the linear plots (in all four cases) of $\ln(x_e/(x_e - x)) = f(t)$ (where x and x_e are the percentages of the isomer **1b** before and at the point when the thermodynamic equilibrium was reached, respectively) and from the thermodynamic equilibrium constant. The linear Eyring plots of the isomerization rate constants in Figure 1 afforded the activation parameters $\Delta H^{\ddagger}_{1a\rightarrow 1b} = 18.5\ (\pm 2)$ kcal mol^{-1} ($\Delta S^{\ddagger} = -7\ (\pm 1)$ eu) and $\Delta H^{\ddagger}_{1b\rightarrow 1a} = 18.4\ (\pm 2)$ kcal mol^{-1} ($\Delta S^{\ddagger} = -11\ (\pm 1)$ eu). These values are somewhat higher than those measured for other trinuclear metal–alkyne clusters.[12] They account for the fact that the alkyne does not rapidly alternate between the faces of the Fe_3 triangle. We will not speculate on why **1a** and **1b** have high interconversion barriers, but it is interesting to note that the alkyne present in these conformers has strong electron-withdrawing substituents.

Thermal Substitution of Tertiary Phosphite and Phosphine for CO in 1: Kinetic Analysis. The coordination mode of an alkyne to a triangular metal cluster has been shown to be strongly dependent on the back-donation ability from the metal atoms to the alkyne.[2c,4] When the back-donating effect increases, the cluster is inclined to adopt a 46-electron configuration. In order to check whether the presence of one monodentate phosphine or phosphite ligand on the alkyne–iron framework would be sufficient to induce some change in the alkyne orientation within the organometallic skeleton, we treated the parent cluster **1** with PMe_3 and $P(OMe)_3$.

The replacement of CO with trimethylphosphine or trimethyl phosphite for $[Fe_3Cp_2(CO)_5(CF_3C_2CF_3)]$ (**1**) occurred quite readily in $CDCl_3$ at about 60 °C (2.5 h), affording the monosubstituted complexes $[Fe_3Cp_2(CO)_4(PMe_3)(CF_3C_2CF_3)]$ (**2**) and $[Fe_3Cp_2(CO)_4\{P(OMe)_3\}(CF_3C_2CF_3)]$ (**3**), respectively, in good yields (Scheme 2). No disubstituted compound was detected even when a large excess of phosphine was used. The ^{19}F NMR spectrum of **3** shows signals consistent with the presence of two isomers in equilibrium in solution, whereas that of **2** indicates the presence of only one isomer. The **3a**:**3b** ratio is not affected by the temperature but depends on the solvent ($CDCl_3$, **3a**:**3b** = 49:1). The complexes **2** and **3** have been characterized by NMR and IR spectroscopy (see Experimental Section). The data show that the structures contain a semibridging carbonyl ligand, a μ_3-CO ligand, and two terminal CO groups. A change of the alkyne orientation on the organometallic skeleton from parallel ($\eta^2(\|)$) to perpendicular ($\eta^2(\perp)$) as a result of the substitution in **1** of one CO by a more basic ligand would imply the loss of an additional carbonyl group in order to obtain a 46-electron configuration. Now spectral data show the existence of four remaining carbonyl ligands in **2** and **3**, which excludes a perpendicular coordination mode of the alkyne, since this mode is exclusively observed in 46-electron clusters. Thus, the data are consistent with a μ^3-$\eta^2(\|)$ coordination mode of the alkyne, analogous to that found for the parent cluster **1**. NMR data for **2** and the major isomer **3a** are in accordance with the asymmetric structure shown in Scheme 2. By subtracting from the ^{19}F NMR spectra of **3** the peaks belonging to **3a**, we get the spectral pattern of **3b**, which shows only one signal at −51.6 ppm, which is consistent with a symmetrical structure (Scheme 2). Indeed, according to this, a closo trigonal-bipyramidal configuration (μ_3-$\eta^2(\perp)$) could be ruled out for **3b**, since in such a geometry the CF_3 groups of the alkyne should be nonequivalent. Substitution of CO ligands effected under thermal conditions often leads to mixtures of mono- and polysubstituted derivatives, but we notice that here the substitution reaction is highly regioselective. According to the value of the coupling constant between the phosphorus and fluorine atoms ($^4J_{F-P}$ = 5 Hz), it appears that the CO ligand replaced in the parent cluster was *trans* to the CF_3 group.

In an attempt to examine the mechanism of ligand substitution for these triiron clusters, we studied the kinetics of the reactions of **1** with PMe_3 and $P(OMe)_3$ (Scheme 2). Rates for the reaction of **1** (0.2 M) in $CDCl_3$ with a stoichiometric amount of PMe_3 or $P(OMe)_3$ were calculated by monitoring the time dependence of the ^{19}F NMR spectra of either the starting material or the products, at five temperatures. The rate of disappearance of the triiron complex **1** was fitted to a second-order rate law. This can be seen from the linear plots (in all five

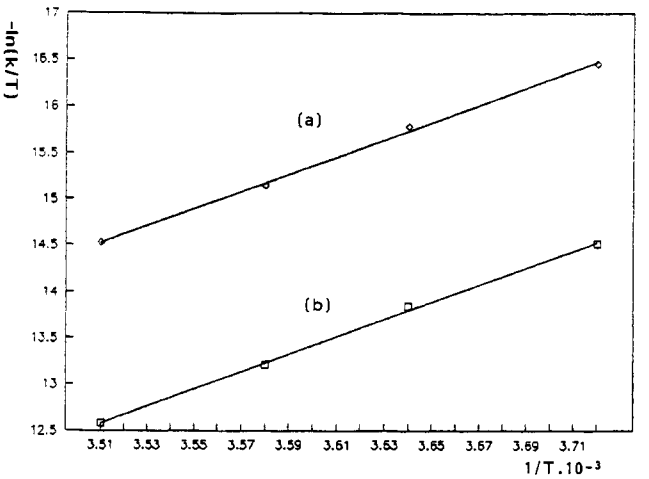

Figure 1. Eyring plots of (a) $-\ln(k/T)$ vs $T^{-1} \times 10^{-3}$ or (b) $-\ln(k_{-1}/T)$ vs $T^{-1} \times 10^{-3}$ for the **1a–1b** isomerization reaction.

Scheme 2

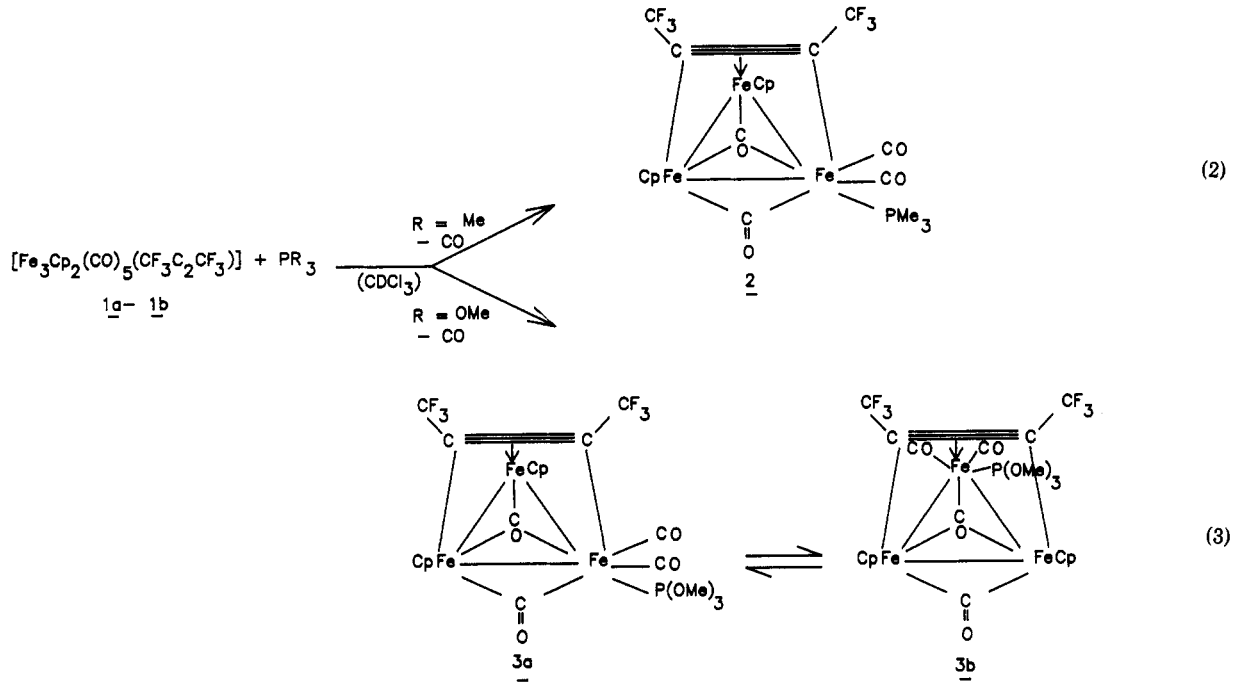

(2)

(3)

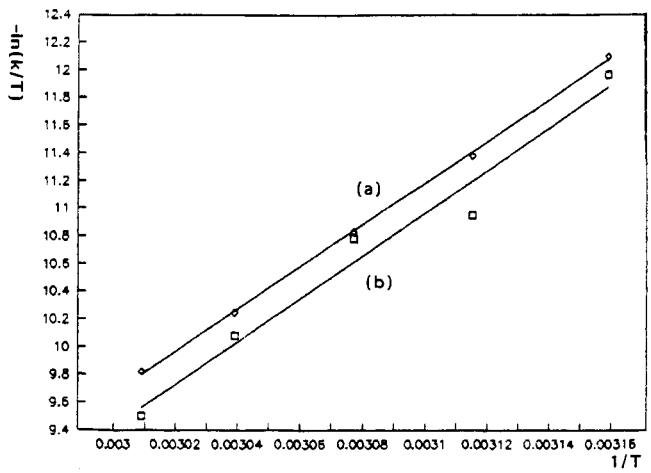

Figure 2. Eyring plots of $-\ln(k/T)$ vs T^{-1} for reaction of 1 with (a) PMe_3 or (b) $P(OMe)_3$.

Table 2. Temperature Dependence of k for the Substitution of CO by (a) PMe_3 or (b) $P(OMe)_3$ on 1 (0.2 M) in $CDCl_3$

a		b	
temp, K	10^3k, L mol^{-1} s^{-1}	temp, K	10^3k, L mol^{-1} s^{-1}
316.5	1.76	316.5	2.0
321	3.66	321	5.6
325	6.44	325	6.75
329	11.66	329	13.8
332.3	18.00	332.3	25.0

cases) of 100/(100 − x) (where x is the percentage of the product 2 or 3) vs time: k_{obsd} was obtained from the slopes of such plots. The rate constants for the disappearance of 1 are given in Table 2. The linear Eyring plot of the exchange rate constants in Figure 2 afforded the activation parameters $\Delta H^{\ddagger}_{1\to2}$ = 30.0 (±1) kcal mol^{-1} ($\Delta S^{\ddagger}$ = 24 (±1) eu) and $\Delta H^{\ddagger}_{1\to3}$ = 30.6 (±1) kcal mol^{-1} ($\Delta S^{\ddagger}$ = 26 (±1) eu). The kinetic results concerning the reactions 2 and 3 (Scheme 2) rule out a dissociative substitution pathway for these compounds and establish the associative nature of the substitution process. Thus, the replacement of carbon monoxide in reactions 2 and 3 involves both variable bonding capabilities of one carbonyl ligand and iron–iron bond scission to expose a coordinatively unsaturated 16-electron iron center, which is followed by rapid association with the nucleophile to afford the monosubstituted products. This stepwise sequence depicted in Scheme 3 does not involve the formation of a 20-electron intermediate. A possible substitution process involving alkyne π decoordination seems very unlikely, since this would imply that the replacement of CO by phosphine or phosphite in 1a, for example, occurs at the unsaturated 16-electron CpFe center; this is not observed experimentally. The values of the activation enthalpy of complexes 2 and 3 are very similar and are high compared with those of other cluster metal carbonyls,[13] which suggests that for this S_N2 process there is more bond breaking than bond making in the formation of the active intermediate (Scheme 3). This also should explain the positive value of the activation entropy.

In conclusion, the presence in the triiron cluster of one phosphine or a ligand, which is a better σ donor than a carbonyl ligand, is not sufficient to induce the rotation of the alkyne over the metallic triangle in order to obtain the $\eta^2(\perp)$ coordination mode from the $\eta^2(\parallel)$ one. This emphasizes the role of the substituents on the alkyne on the coordination mode of an alkyne to M_3 clusters. Thus, with strong electron-withdrawing groups (e.g. CF_3) as substituents on the alkyne the electronegativity of the metals should need to be lower than that of iron atoms, in order to stabilize a perpendicular orientation of the alkyne. This is confirmed by the results obtained for bidentate phosphine ligands (L = dppm, dppe), whose reactions with $[Fe_3Cp_2(CO)_5(CF_3C_2CF_3)]$ (1) gave only the saturated 48-electron complexes $[Fe_3Cp_2(CO)_4(L)(CF_3C_2CF_3)]$, with no evidence for corresponding unsaturated species.[14] Such an observation agrees with the work of Smith et al.,[15] who have shown recently that the reaction

(13) Basolo, F. *Inorg. Chim. Acta* **1985**, *100*, 33 and references cited therein.

(14) Robin-Le Guen, F.; Rumin, R.; Pétillon, F. Y. To be submitted for publication.

Scheme 3

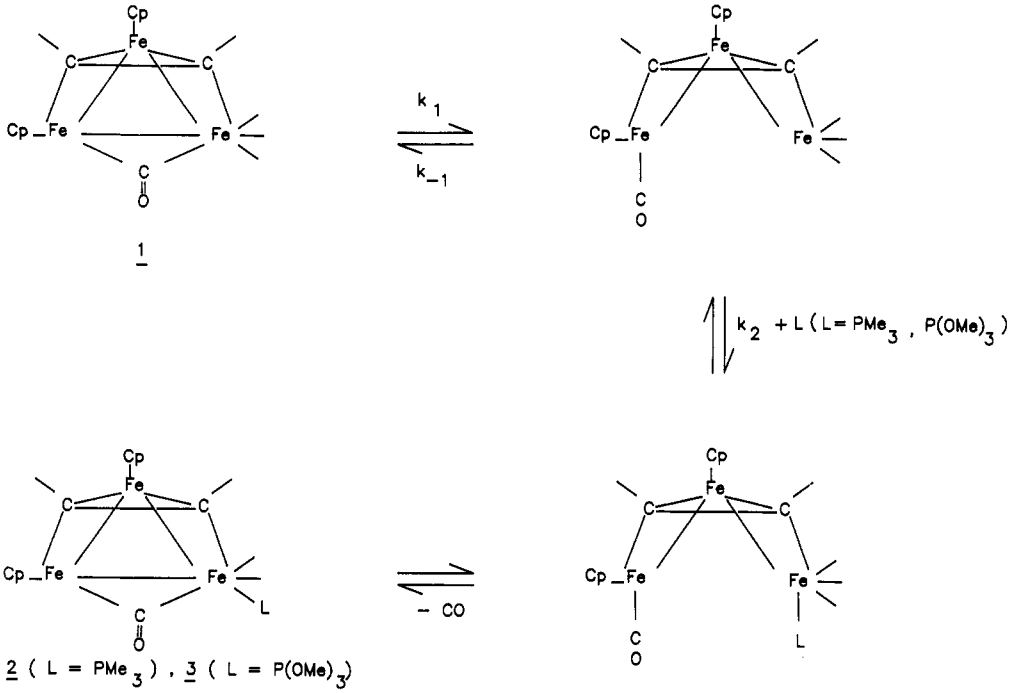

Table 3. Redox Potentials[a] of Clusters 1-3 As Measured by Cyclic Voltammetry in THF-(Bu_4N)(PF_6)

			first redox process		second process		
cluster	L	solvent	E_{pred1} ($E_{p/2}$)	$E^{1/2}_{ox1}$	$E^{1,2}_{red}$	E_{pox}	$E^{1/2}_{ox}$
1a	CO	THF	−1.44 (1.36)	0.60	−1.95	−1.51	−0.92
		MeCN	−1.29 (−1.23)		−1.63	−1.35	−0.86 ($E_{p/2}$ = −0.92)
1b	CO	THF	−1.18 ($E^{1/2}$)				
		MeCN	−1.12 ($E^{1/2}$)				
2	PMe_3	THF	−1.75 (−1.67)	0.23	−1.94	−1.53	−0.92
3	$P(OMe)_3$	THF	−1.68 (−1.62)	0.25	−1.94	−1.53	−0.92

[a] All potentials are in V vs the ferrocene/ferrocenium couple.

of the triosmium cluster $[Os_3(\mu\text{-H})(CO)_8\{Ph_2PCH_2P(Ph)(C_6H_4)\}]$ with alkynes RC_2R gave a μ_3-$\eta^2(\|)$ mode when R is an electron-attracting group (CF_3) and a μ^3-$\eta^2(\perp)$ mode when R = Ph. The triiron clusters described here are the first examples of triiron compounds exhibiting a parallel orientation of the alkyne with respect to a metal–metal bond, in spite of the low electronegativity of the metal. The replacement of one CO ligand in the triiron cluster **1** by a phosphane group favors the asymmetrical $\eta^2(\|)$ structure, since the **3a:3b** ratio (49:1) was high compared to **1a:1b** one (7:1). Moreover, when the trimethylphosphine is used, only the asymmetrical isomer was obtained. This result is quite surprising, since the replacement of one CO by the more basic ligand (here PMe_3) stabilizes the asymmetrical structure, which is in disagreement with theoretical previsions.[2b] This observation shows once more that prediction of alkyne orientation within a trimetallic framework must take into account the influence of the substituents of the alkyne.

Electrochemical Investigations. Our previous electrochemical studies on a "Fe_2SC_2" cluster have shown that its reduction results in the decoordination of a CO group. Such a reaction associated with a change in the electron richness of the metal centers as a result of the reduction of clusters **1–3** might induce a rotation of the alkyne over the Fe_3 triangle. Therefore, we have investigated the electrochemical behavior of clusters **1–3** in THF– and MeCN–electrolyte mixtures.

First Reduction of Clusters 1a, 2, and 3 and the Coupled Chemical Step. The cyclic voltammetry (CV) of clusters **1a**, **2**, and **3** (room temperature, N_2 atmosphere, THF-(Bu_4N)(PF_6) electrolyte) displays a reversible (or quasi-reversible for **1a**) one-electron oxidation and an irreversible one-electron reduction. The potentials for the first redox processes (Table 3) are sensitive to the substitution of the donor ligand PMe_3 or $P(OMe)_3$ for CO. The irreversibility of the first reduction should be assigned to the occurrence of a fast chemical step after the electron transfer (EC process) rather than to a slow heterogeneous electron transfer rate. This is confirmed by the low temperature CV of **1a** in MeCN–electrolyte: under these conditions the first reduction of **1a** shows reversibility and a second, irreversible, reduction is also observed (E_{pred2} = −2.13 V) (Figure 3). As evidenced by the CV in Figures 4 and 5, the same product ($P_1^{\bullet-}$), characterized by the redox processes at $E^{1/2}_{ox}$ = −0.92 V and $E^{1/2}_{red}$ = −1.94 V (THF electrolyte; in MeCN, the potentials are E_{pox} = −0.86 V (irreversible oxidation, $E_{p/2ox}$ = −0.92 V) and $E^{1/2}_{red}$ = −1.63 V, respectively), arises from the EC reduction of complexes **1a** and **3**. This is also the case for cluster **2**. It is therefore clear that the one-electron reduction of clusters **1a**, **2**, and **3** is followed by the rapid loss of a ligand, *e.g.* CO, PMe_3, and $P(OMe)_3$, respectively (reaction 4).

Controlled-potential electrolyses of the clusters at the potential of their first reduction in a THF electrolyte are

(15) Brown, M. P.; Dolby, P. A.; Harding, M. M.; Mathews, A. J.; Smith, A. K.; Osella, D.; Arbrun, M.; Gobetto, R.; Raithby, P. R.; Zanello, P. *J. Chem. Soc., Dalton Trans.* **1993**, 827.

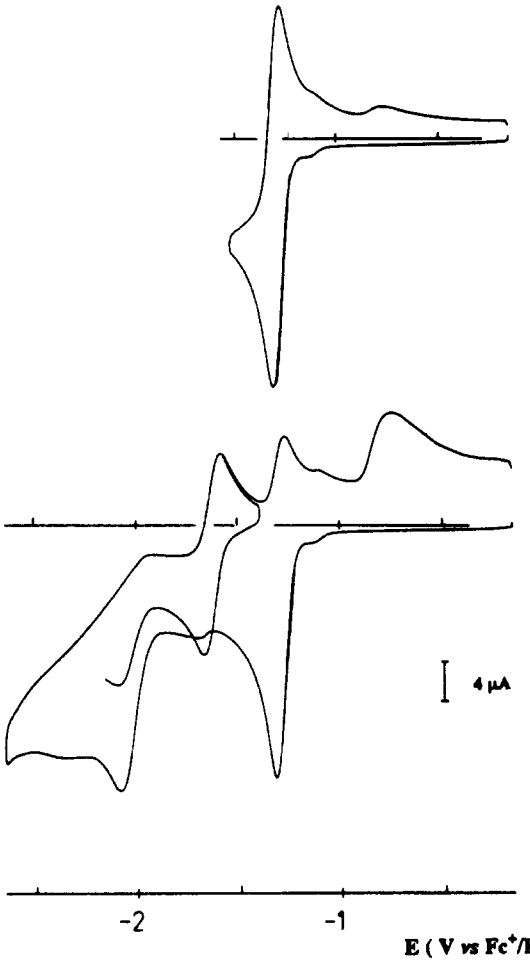

Figure 3. Low-temperature cyclic voltammetry of a 1.3 mM solution of **1a** in MeCN–$(Bu_4N)(PF_6)$ (T = –30 °C; vitreous carbon electrode; v = 0.2 V/s). The reversible system shown on the reverse scan corresponds to the $P_1^{2-}/P_1^{\bullet-}$ couple (see text).

$$\underset{48\text{ e}}{\mathbf{1a, 2, 3}} \xrightarrow{e^-} \underset{47\text{ e}}{P_1^{\bullet-}} + L \qquad (4)$$

$$L = CO, PMe_3, P(OMe)_3$$

completed after *ca.* 1 F/mol of starting material has passed. CV monitoring of the course of the electrolysis shows a linear decay of the first reduction peak current with the charge consumed and a steady increase of the oxidation peak of $P_1^{\bullet-}$. The yield of $P_1^{\bullet-}$, calculated from the comparison of its oxidation peak current to that of the starting material before electrolysis, is *ca.* 55%. The bulk electrolyses of **1a**, **2**, and **3** also result in the formation of variable amounts of a byproduct with $E^{1/2}_{red}$ = –1.3 V: this product has been characterized by ^1H and ^{19}F NMR and IR spectroscopy and CV as the already known[21] $[CpFe(\mu\text{-}CO)_2\{\mu\text{-}(CF_3C_2CF_3)\}FeCp]$ complex (**4**). The formation of this fragment requires that some decomposition product $\{Fe(CO)_n\}^{m-}$ be generated as well. As **4** is electroactive at the same potential as **1a**, the coulometric experiments were more conveniently carried out on solutions of **2** or **3**.

Our attempts to isolate $P_1^{\bullet-}$ from the solution after bulk electrolyses of clusters **1a**, **2**, and **3** under N_2 (THF–$LiClO_4$ electrolyte) failed. The only products characterized after workup were the starting material and the dinuclear complex $[CpFe(\mu\text{-}CO)_2\{\mu\text{-}(CF_3C_2CF_3)\}FeCp]$ (**4**), although

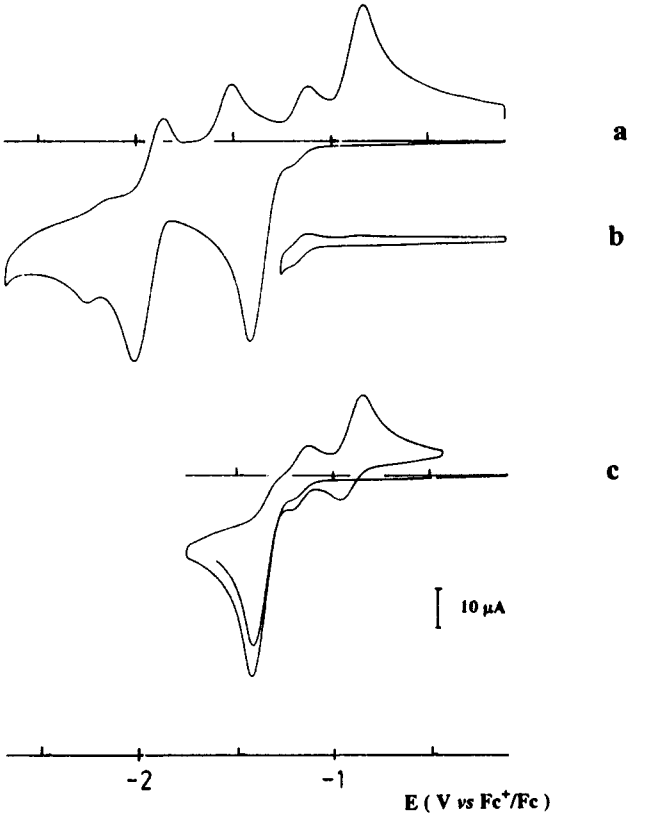

Figure 4. Cyclic voltammetry of a 2 mM solution of **1a** in THF–$(Bu_4N)(PF_6)$ (vitreous carbon electrode; v = 0.2 V/s).

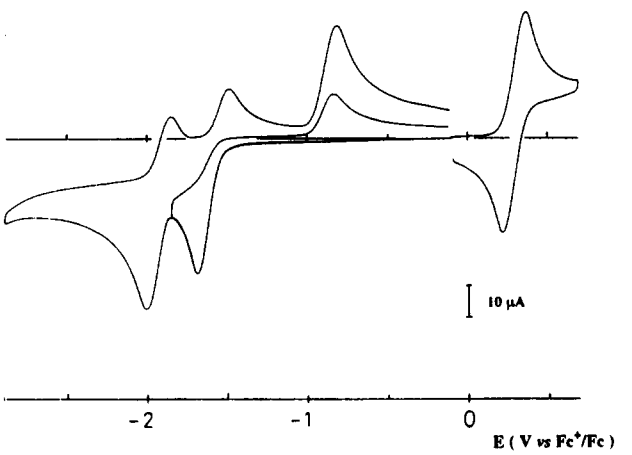

Figure 5. Cyclic voltammetry of a 1.8 mM solution of **3** in THF–$(Bu_4N)(PF_6)$ (vitreous carbon electrode; v = 0.2 V/s).

CV of the catholyte clearly showed that $P_1^{\bullet-}$ had formed (see Experimental Section).

We have also attempted to isolate the neutral P_1 species: the radical anion resulting from the controlled-potential reduction of **1a** was electrochemically oxidized at –0.7 V. However, the major product of the oxidation, characterized by a reversible reduction at –1.3 V, is the dinuclear complex **4**. After workup, NMR analysis of the mixture of products shows that the distribution of **1a** and **4** is 26:64. Therefore, it appears that P_1 has only a limited kinetic stability (eq 5).

$$P_1^{\bullet-} \underset{+e^-}{\overset{-e^-}{\rightleftharpoons}} P_1 \rightarrow 4 + \text{products} \qquad (5)$$

Electron-Transfer Chemistry and Chemical Reactivity of the Reduction Product. Electron-Transfer

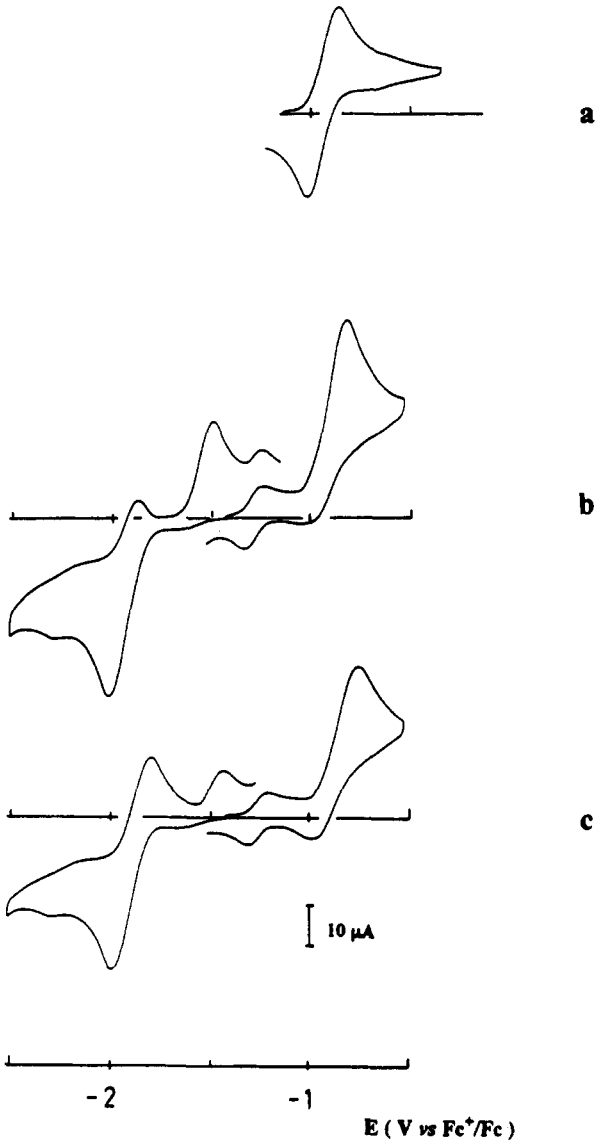

Figure 6. Cyclic voltammetry of the catholyte after controlled-potential reduction of (a) a 2 mM solution of **1a** (reduction potential 1.6 V; Hg-pool cathode; 0.8 F/mol of **1a**) showing the reversible oxidation of $P_1^{\bullet-}$ and (b) a 4 mM solution of **3** (reduction potential −1.7 V; Hg-pool cathode; 1.2 F/mol of **3**). The CV in (c) is the same as in (b) but recorded at the temperature of −25 °C and shows the quasi-reversible reduction of $P_1^{\bullet-}$ and the suppression of the irreversible oxidation peak of P_2^{2-} (THF–$(Bu_4N)(PF_6)$) (vitreous carbon electrode; v = 0.2 V/s).

Reactions of the Reduction Product. The oxidation and the reduction of $P_1^{\bullet-}$ both occur according to EC processes. The oxidation of $P_1^{\bullet-}$ in the presence of a ligand L (THF–electrolyte)[16] regenerates the parent clusters **1a**, **2**, and **3** (L = CO, PMe_3, $P(OMe)_3$, respectively). Our evidence for this is as follows: the oxidation couple at $E^{1/2}{}_{ox}$ = −0.92 V in Figure 4c shows a cathodic to anodic peak current ratio less than unity: this is because the CO released in the electrode vicinity as a consequence of the EC reduction of **1a** (reaction 4) reacts with P_1 to regenerate the starting material. When it is generated from the bulk electrolysis of cluster **1a** (under N_2, the CO released on reduction is removed from the solution), $P_1^{\bullet-}$ shows a chemically reversible oxidation on the CV time scale (Figure 6a). On the other hand, since the $P(OMe)_3$ ligand released during the controlled-potential reduction of **3** remains in the solution, the oxidation of $P_1^{\bullet-}$ generated under these conditions appears as a poorly reversible system: the EC oxidation of $P_1^{\bullet-}$ at −0.92 V regenerates the starting material **3**, as evidenced by the detection of its reversible oxidation at 0.25 V on the positive scan while its reduction process is completely absent. This can be summarized as shown in Scheme 4.

Scheme 4

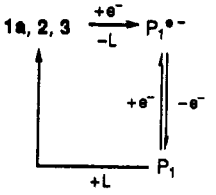

1a: L = CO
2: L = PMe_3
3: L = $P(OMe)_3$

Scheme 5[a]

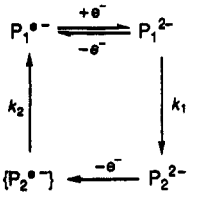

$k_2 >> k_1$

[a] $\{P_2^{\bullet-}\}$ is not detected by CV.

The reduction couple of $P_1^{\bullet-}$ also presents the characteristics of a system that is not fully reversible chemically ($(i_p^a/i_p^c)_{red} < 1$). The irreversible oxidation peak at E_{pox} = −1.53 V (Figure 6b) is assigned to a product (P_2^{2-}) arising from the decay of the dianion P_1^{2-} (Scheme 5), since it is suppressed at lower temperature when the redox couple $P_1^{\bullet-}/P_1^{2-}$ is chemically more reversible (Figure 6c). At room temperature, the oxidation of P_2^{2-} leads to the regeneration of $P_1^{\bullet-}$, $P_2^{\bullet-}$ not being detected by CV (v < 1 V/s); this suggests that the chemical step involving $P_2^{\bullet-}$ is faster than the chemical transformation of P_1^{2-} into P_2^{2-} (Scheme 5).

Reaction of the Reduction Product with Carbon Monoxide. In addition to the chemistry coupled to the electron-transfer steps of $P_1^{\bullet-}$, the radical anion is also involved in a reaction with carbon monoxide, which leads to the minor isomer of **1a**. In the CV of **1a**, a small reversible couple ($E^{1/2}{}_{red}$ = −1.18 V) is detected just anodic of the major reduction peak (Figure 4b); this process, which is not observed when the CV is run immediately after the cluster has been dissolved in the THF–electrolyte mixture, is assigned to the reduction of the minor isomer of **1a**, *e.g.* **1b**. The cathodic current for this couple accounts for 10–15% of the total reduction current, and this is in agreement with the calculated percentage of the minor isomer of **1a** (see above). The increase in the peak currents for this system from Figure 4b to Figure 4c makes clear that some isomerization occurred during the reduction of **1a**. The increase in the ratio of the oxidation peak currents of $P_1^{\bullet-}$ and $\mathbf{1b}^{\bullet-}$ at −0.92 and −1.18 V, respectively, as the scan rate is increased from 0.02 to 1 V/s suggests that $P_1^{\bullet-}$ is

(16) Bard, A. J.; Faulkner, L. R. In *Electrochemical Methods: Fundamentals and Applications*; Wiley: New York, 1980; p 429.

(17) The anodic to cathodic peak separation for the $\mathbf{1b}/\mathbf{1b}^{\bullet-}$ couple is *ca.* 60 mV in MeCN (ΔE_p for ferrocene is also 60 mV). In MeCN, the $P_1/P_1^{\bullet-}$ couple is not reversible.

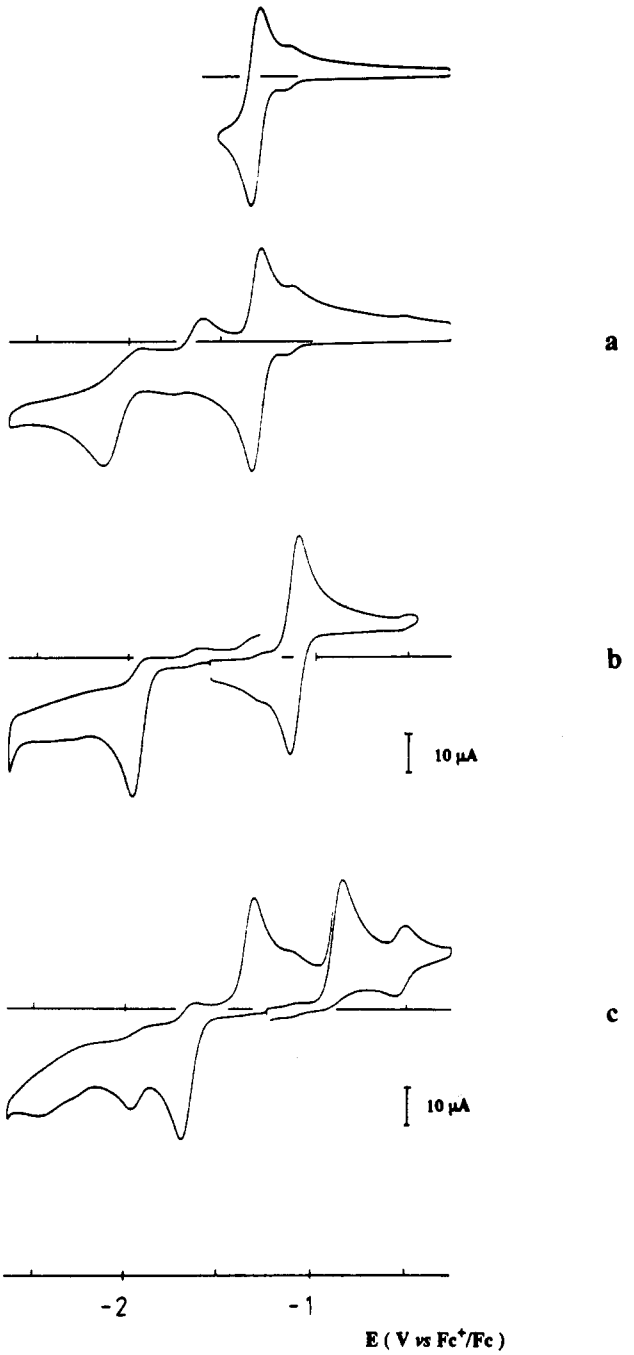

Figure 7. Cyclic voltammetry of a 1.6 mM solution of **1a** in a MeCN-$(Bu_4N)(PF_6)$ electrolyte (a) under CO at low temperature (T *ca.* −30 °C), (b) after controlled-potential reduction at −30 °C under CO, showing the redox processes of $\mathbf{1b}^{\bullet-}$ (Hg-pool cathode; reduction potential −1.45 V; 1 F/mol of **1a**), and (c) after purging the solution corresponding to (b) with N_2, showing the conversion $\mathbf{1b}^{\bullet-} \rightarrow P_1^{\bullet-}$ (vitreous carbon electrode; v = 0.2 V/s).

an intermediate on the pathway to $\mathbf{1b}^{\bullet-}$. The conversion of $P_1^{\bullet-}$ into $\mathbf{1b}^{\bullet-}$ is quantitative when the reduction of **1a**, but also that of **2** and **3**, is run under a CO atmosphere: under these conditions, the oxidation couple $P_1^{\bullet-}/P_1$ is replaced by the $\mathbf{1b}^{\bullet-}/\mathbf{1b}$ oxidation system. Controlled-potential electrolyses of **1a** have been performed under a CO atmosphere in a THF–electrolyte mixture at the potential of the primary reduction: the electrolysis produces *ca.* 40% (calculated from CV peak current measurements) of $\mathbf{1b}^{\bullet-}$ along with unidentified degradation products. These experiments were repeated at low temperature (under CO) in a MeCN electrolyte and, although $\mathbf{1a}^{\bullet-}$ appears stable on the CV time scale under these conditions (Figure 7a), the controlled-potential reduction at the first wave results in the formation of 95–97% (CV measurement) of $\mathbf{1b}^{\bullet-}$ (Figure 7b). When the solution is purged with N_2, $\mathbf{1b}^{\bullet-}$ is converted to $P_1^{\bullet-}$ (Figure 7c), and this reaction is reversible since $\mathbf{1b}^{\bullet-}$ is regenerated under CO. Therefore, the irreversible loss of CO from $\mathbf{1a}^{\bullet-}$ appears as a much faster reaction that the reversible decarbonylation of $\mathbf{1b}^{\bullet-}$.

Scheme 6[a]

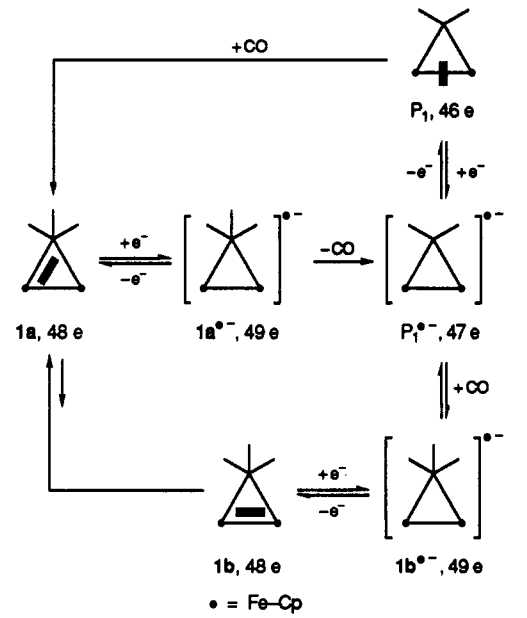

[a] The orientation of the alkyne in the ionic species is not indicated.

Influence of the Electron Count on the Orientation of the Alkyne Ligand above the Fe_3 Triangle. Although we have not been able to isolate the reduction product $P_1^{\bullet-}$ of clusters **1a**, **2**, and **3**, the electrochemical experiments reported above indicate that it must retain the triangular metal framework of its precursors, as well as the alkyne ligand. The fact that the $P_1/P_1^{\bullet-}$ and $\mathbf{1b}/\mathbf{1b}^{\bullet-}$ couples appear almost electrochemically reversible with ΔE_p of *ca.* 100–110 mV in THF[17] (compare with ΔE_p = 90 mV for ferrocene under the same conditions) suggests that there is no important reorientation of the alkyne as a result of the electron transfer step itself; however, the charge of the cluster framework is crucial as to the orientation of the alkyne after CO loss or CO addition. This is shown by the fact that the reaction of CO with each partner of the $P_1/P_1^{\bullet-}$ couple produces different isomers (neutral and reduced, respectively) of the clusters: $\mathbf{1b}^{\bullet-}$ is generated from the reaction of $P_1^{\bullet-}$ with CO, whereas the starting materials **1a**, **2**, and **3** are regenerated from the reaction of P_1 with CO, PMe_3, or $P(OMe)_3$ respectively (Scheme 6). In other terms, the oxidation of $P_1^{\bullet-}$ followed by reaction with CO (*EC* process) produces **1a**, whereas reaction of $P_1^{\bullet-}$ with CO, followed by the oxidation of the product (*CE* process), leads to **1b**. This behavior differs strongly from that reported by Smith et al.,[15] who detected an electrochemically irreversible system for the two-electron transfer $[Os_3(CO)_7(PhC_2Ph)(Ph_2PCH_2PPh_2)] \rightarrow [Os_3(CO)_7(PhC_2Ph)(PhPCH_2PPh_2)]^{2-}$, which they assigned to the $\perp$–$\parallel$ reorientation within the triosmium framework.

The formation of **4** (with the alkyne perpendicular to the metal–metal bond) from the reduction of clusters **1a**, **2**, and **3** in a THF electrolyte might also indicate that, in its precursors P_1 or $P_1^{\bullet-}$, the alkyne ligand is already perpendicular to the CpFe–FeCp bond. It is therefore reasonable to infer that P_1, which has one CO group less than **1a**, has a closo geometry.

These results also show that the preferred orientation of the alkyne in the nido geometry is reversed in the cluster radical anions: the reduced form of **1a**, **2**, and **3** is highly labile and is only detected by low-temperature CV (Figure 3), whereas $\mathbf{1b}^{\bullet-}$ appears to be stable under a CO atmosphere.

Conclusions

Our investigations have shown that the coordination mode of an alkyne to triangular metal clusters is highly dependent on both the metal and the substituents of the alkyne. While with a triiron framework a perpendicular coordination mode is expected, a parallel mode is observed when strong electron-withdrawing substituents are present in the alkyne. Kinetic analysis of the asymmetrical **1a**–symmetrical **1b** isomerization suggests a process involving rotation of the alkyne ligand within the triangle through an unsaturated 46-electron species. The barriers of the alkyne rotation in **1** are high compared to those calculated for similar processes.[12] Reaction of tertiary phosphane with **1** gave rise to the monosubstituted products $[Fe_3Cp(CO)_4L(CF_3C_2CF_3)]$ (**2**, **3**), where the alkyne ligand is parallel to an iron–iron axis, which demonstrates that the presence of a more basic ligand in the cluster is not sufficient to induce a reorientation of the alkyne from parallel to perpendicular.

The electrochemical behavior parallels that observed by thermal activation and shows also that **1a**–**1b** isomerization involves an intermediate where the alkyne has a μ_3-$\eta^2(\perp)$ mode of coordination. Interestingly, the electrochemical data suggest that the reorientation of the alkyne within the triiron compounds depends on the charge of the cluster framework but does not result from the electron transfer step itself.

Experimental Section

The chemical, electrochemical, and kinetic experiments were carried out under an inert atmosphere (dinitrogen or argon) in carefully deaerated solvents.

Infrared spectra were obtained with a Perkin-Elmer 1430 spectrometer in hexane solutions in the ν(CO) region. NMR spectra (^{1}H, ^{13}C, ^{19}F, ^{31}P), in $CDCl_3$ solutions, were recorded on a JEOL FX100 or a Bruker AC300 at 20 °C in chloroform-*d* and were referenced to Me_4Si, Me_4Si, $CFCl_3$, and H_3PO_4, respectively. Chemical analyses were performed by the "Centre de Microanalyses du CNRS de Lyon". The electrochemical apparatus, the cell, and the electrodes were as described previously.[11]

The triiron cluster $[Fe_3Cp_2(CO)_5(CF_3C_2CF_3)]$ (**1**) was obtained as reported previously.[21]

Preparation of $[Fe_3Cp_2(CO)_4(PMe_3)(CF_3C_2CF_3)]$ (2) and $[Fe_3Cp_2(CO)_4\{P(OMe_3)\}(CF_3C_2CF_3)]$ (3). Phosphane L (L = PMe_3, $P(OMe)_3$) (0.10 mmol) was added to a chloroform-*d* solution of $[Fe_3Cp_2(CO)_5(CF_3C_2CF_3)]$ (**1**) (0.06 g, 0.10 mmol) with stirring at 50 °C (L = PMe_3) or 60 °C (L = $P(OMe)_3$). After 2 h (L = PMe_3) or 3 h (L = $P(OMe)_3$) the red solution was evaporated to dryness and purified by chromatography on a silica gel column. Elution with CH_2Cl_2–hexane (1:1) gave a red band of compound **2** or **3** (yields ~98%).

2. Anal. Calcd for $C_{21}H_{19}F_6Fe_3O_4P$: C, 38.9; H, 2.9. Found: C, 39.0; H, 3.1. IR: ν(CO) 2024 (s), 1974 (s), 1846 (m), 1663 (m) cm^{-1} (hexane). ^{1}H NMR ($CDCl_3$): δ 4.98 (s, 5H, Cp), 4.75 (s, 5H, Cp), 1.34 (d, 9H, J_{PH} = 9 Hz, PMe_3). $^{31}P\{^1H\}$ NMR ($CDCl_3$): δ 12.51 (q, $^4J_{PF}$ = 2.4 Hz). ^{19}F NMR ($CDCl_3$): δ −49.90 (q, 3F, J_{FF} = 13 Hz), −48.48 (dq, 3F, J_{FF} = 13 Hz, $^4J_{PF}$ = 2.4 Hz). $^{13}C\{^1H\}$ NMR ($CDCl_3$): δ 289.8 (d, $^2J_{CP}$ = 8 Hz, μ_3-*C*O), 233 (d, $^2J_{CP}$ = 6 Hz, μ-*C*O), 215.9 (dq, $^2J_{CP}$ = 15 Hz, $^4J_{CF}$ = 1.5 Hz, *C*O), 211 (dq, $^2J_{CP}$ = 23 Hz, $^4J_{CF}$ = 2 Hz, *C*O), 164.7 (q qui, $^2J_{CF}$ = 35 Hz, $^3J_{CF}$ = $^3J_{CP}$ = 3.5 Hz, *C*(CF_3)), 157.2 (dqq, $^2J_{CF}$ = 36 Hz, $^2J_{CP}$ = 16 Hz, $^3J_{CF}$ = 3.5 Hz, *C*(CF_3)), 129.7 (dq, J_{CF} = 276 Hz, $^3J_{CP}$ = 3 Hz, *C*F_3), 129.2 (q, J_{CF} = 276 Hz, *C*F_3), 92.5 (s, *C*$_5H_5$), 87.2 (s, *C*$_5H_5$), 16.3 (d, J_{CP} = 28 Hz, P(*C*H_3)$_3$).

3. Anal. Calcd for $C_{21}H_{19}F_6Fe_3O_7P$: C, 36.2; H, 2.75. Found: C, 36.2; H, 2.7.

3a. IR: ν(CO) 2031 (s), 1975 (s), 1863 (m), 1683 (m) (hexane). ^{1}H NMR ($CDCl_3$): δ 5.0 (s, 5H, Cp), 4.78 (s, 5H, Cp), 3.78 (d, 9H, J_{PH} = 11 Hz, $P(OMe)_3$). $^{13}P\{^1H\}$ NMR ($CDCl_3$): δ 141.1 (q, $^4J_{PF}$ = 5 Hz). ^{19}F NMR: δ −50.8 (q, 3F, J_{FF} = 12 Hz), −48.70 (dq, 3F, J_{FF} = 12 Hz, $^4J_{PF}$ = 5 Hz). $^{13}C\{^1H\}$ NMR: δ 287.3 (d, $^2J_{CP}$ = 10 Hz, μ_3-*C*O), 230.1 (d, $^2J_{CP}$ = 9 Hz, μ-*C*O), 213.6 (br d, $^2J_{CP}$ = 24 Hz, *C*O), 209.9 (br d, $^2J_{CP}$ = 31 Hz, *C*O), 167 (m, *C*(CF_3)), 156.7 (m, *C*(CF_3)), 129.6 (dq, J_{CF} = 276 Hz, $^3J_{CP}$ = 5 Hz, *C*F_3), 128.4 (dq, J_{CF} = 276 Hz, $^3J_{CP}$ = 3 Hz, *C*F_3), 92.4 (s, *C*$_5H_5$), 87.05 (s, *C*$_5H_5$), 53.25 (d, $^2J_{CP}$ = 8 Hz, $P(OMe)_3$).

3b. ^{19}F NMR ($CDCl_3$): δ −51.6 (s).

Kinetic Measurements. 1a–1b Isomerization Reactions. The kinetic runs were monitored by ^{19}F NMR (99.66 MHz). A 0.2 M solution of triiron complex **1** was prepared by placing 0.060 g of the compound in cooled (213 K) chloroform-*d*. The tube was then inserted into the magnet and taken to the desired temperature. The progress of the reaction was followed by monitoring the decreasing intensity of a typical ^{19}F NMR resonance of **1a** and the increasing intensity of the signal of **1b**. Plots of $\ln(x_e/(x_e - x)) = f(t)$ (where x and x_e are the percentage of **1b** before and at the point when thermodynamic equilibrium was reached, respectively) were linear. The slopes of these lines gave values of k_{obsd}.

CO Substitution in 1 by Tertiary Phosphine. Equilibrium and kinetics studies of the rates of CO substitution were followed by ^{19}F NMR. The reactions were carried out in oxygen-free chloroform-*d* solutions and under conditions where the concentrations of the cluster **1** and that of trimethylphosphine or trimethyl phosphite are the same (in a typical experiment, the concentrations were 0.2 M). The kinetics of the reactions were followed by monitoring the increasing intensity of a typical ^{19}F NMR resonance of the product (**2**, **3**). Plots of $(100)/(100 - x)$ (x = percentage of product vs time (**2**, **3**)) were linear. The slopes of these lines gave values of k_{obsd}.

Electrochemical Studies. Electrochemical Reduction of Clusters 1–3. Owing to the fact that **4** arising from the reduction of the title clusters is electroactive at the same potential as **1a**, the coulometric experiments are more conveniently conducted on solutions of the phosphorus-substituted molecules. The electrosyntheses of $P_1^{\bullet-}$ were carried out from solutions of any of the three clusters in a THF–$(Bu_4N)(PF_6)$ electrolyte, but those intended to isolate the product were performed in the presence of $LiClO_4$ as the supporting electrolyte. In contrast, the attempted one-pot electrosynthesis of P_1 was conducted on solutions of **1a** in a THF–$(Bu_4N)(PF_6)$ electrolyte.

Electrosynthesis of $P_1^{\bullet-}$. In a typical experiment, 0.032 g of **3** (4.6×10^{-5} mol) was dissolved in 25 mL of THF–$(Bu_4N)(PF_6)$ in the electrochemical cell and electrolyzed at −1.7 V on a Hg-pool cathode under dinitrogen. After 4.5 C (1 F/mol of **3**) CV showed that less than 5% of the starting material was left, whereas the product yield calculated from the peak currents (see text) was 58%. The catholyte was syringed out of the cell, transferred to a Schlenk flask under dinitrogen, and taken down to dryness under vacuum. At this stage of the workup, most of the product is still present as $P_1^{\bullet-}$, as shown by the CV of a THF–(Bu_4N)-

(PF_6) solution of the residue; however, the amount of complex **4** has slightly increased and some (<10% of the initial amount) starting material is also present. Addition of diethyl ether/pentane to the solid affords a purple-red solution which is separated by filtration; after evaporation of the solvents, NMR spectroscopy shows the presence of the starting material (ca. 80%) and **4** (20%), with trace amounts of an unidentified product. CV of the residue (THF–(Bu_4N)(PF_6)) after extraction presents no well-defined peak.

The experiment carried out on 0.0654 g (1.1×10^{-4} mol) of **1a** in a THF–$LiClO_4$ electrolyte leads to results similar to those described above; no $P_1^{\bullet-}$ could be isolated.

Attempted Electrosynthesis of P_1. A solution of 0.050 g (8.3×10^{-5} mol) of **1a** in 25 mL of a THF–(Bu_4N)(PF_6) electrolyte was reduced at −1.5 V on a Hg-pool cathode under dinitrogen. The electrolysis was complete after 0.97 F/mol of **1a** had passed. The catholyte was then purged with dinitrogen for a few minutes in order to remove all dissolved carbon monoxide. CV of the electrolyzed solution showed that $P_1^{\bullet-}$ formed in *ca.* 61% yield along with **4** (8% yield) and an unidentified product with a reversible oxidation at −0.62 V (*ca.* 15%) (the yields result from CV measurement). The potential of the graphite anode was then set up at −0.7 V, and the electrolysis was stopped after the passage of 0.58 F/mol of **1a** initially present in solution (this is consistent with the one-electron oxidation of $P_1^{\bullet-}$ formed in 61% yield). CV of the solution resulting from this oxidation showed the presence of **4** as the major product; as shown by rotating-disk-electrode voltammetry, the small couple at −0.92 V is due to unoxidized $P_1^{\bullet-}$. No P_1 was detected. After a workup similar to that described above, NMR spectroscopy showed the presence of a mixture of **1a** and **4** (26:64) with 10% of an unidentified product.

Acknowledgment. The CNRS and Brest University are acknowledged for financial support.

OM9306887